Electronic Supplementary Information (ESI)

Superhigh out-of-plane piezoelectricity, low thermal conductivity and photocatalytic abilities in ultrathin 2D van der Waals heterostructures of Boron Monophosphide and Gallium Nitride

Manish Kumar Mohanta, Ashima Rawat, Dimple, Nityasagar Jena, Raihan Ahammed and Abir De Sarkar[*]

Institute of Nano Science and Technology, Phase 10, Sector 64, Mohali, Punjab-160062, India
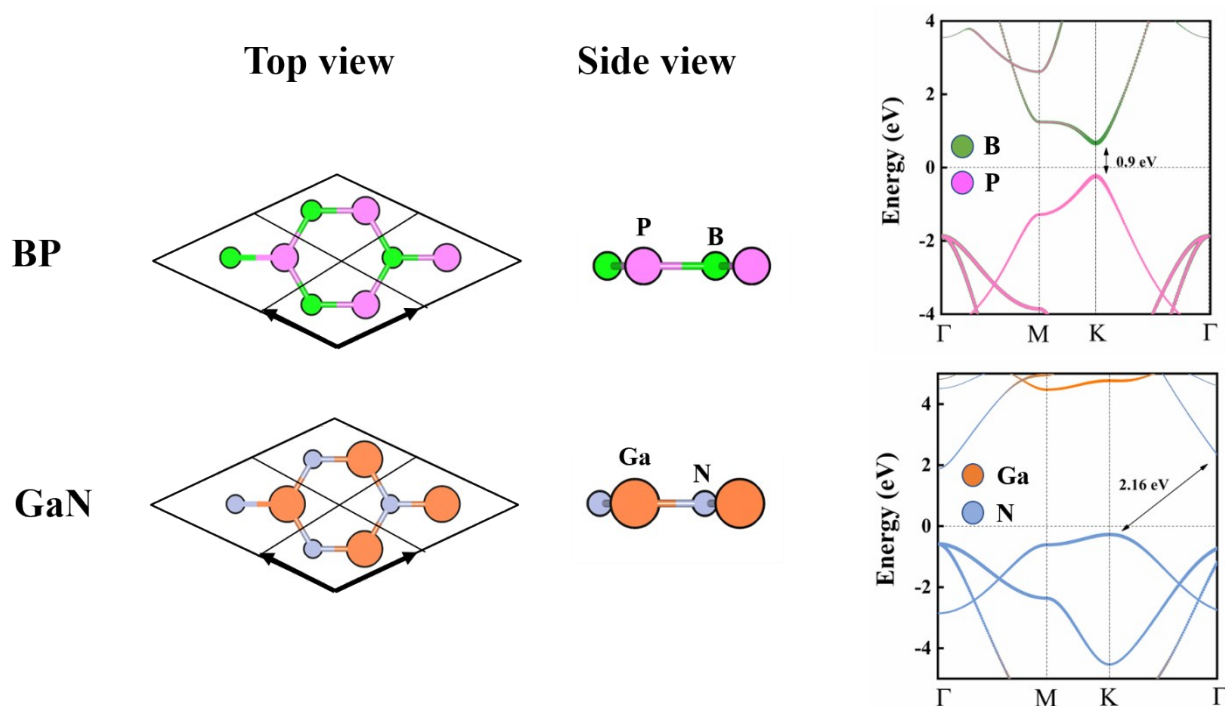
*E-mail: abir@inst.ac.in; abirdesarkar@gmail.com

Fig S1: Top and side view of monolayer GaN and BP along with band structure of pristine monolayers
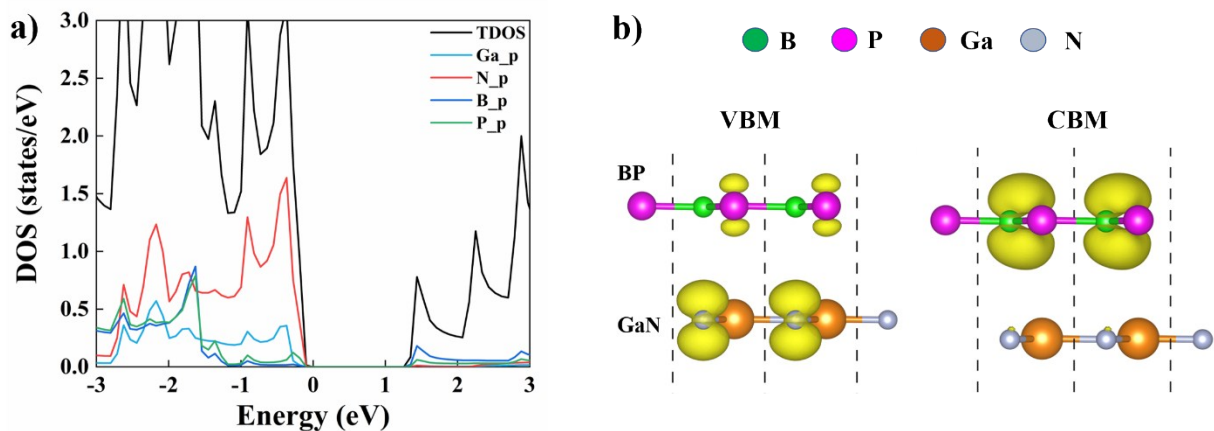
Fig S2: (a) Partial density of states of individual atoms in the heterobilayer (b) Band decomposed charge density of VBM and CBM of BP/GaN heterostructure with the iso-surface of 0.015 e/Å^3 respectively.
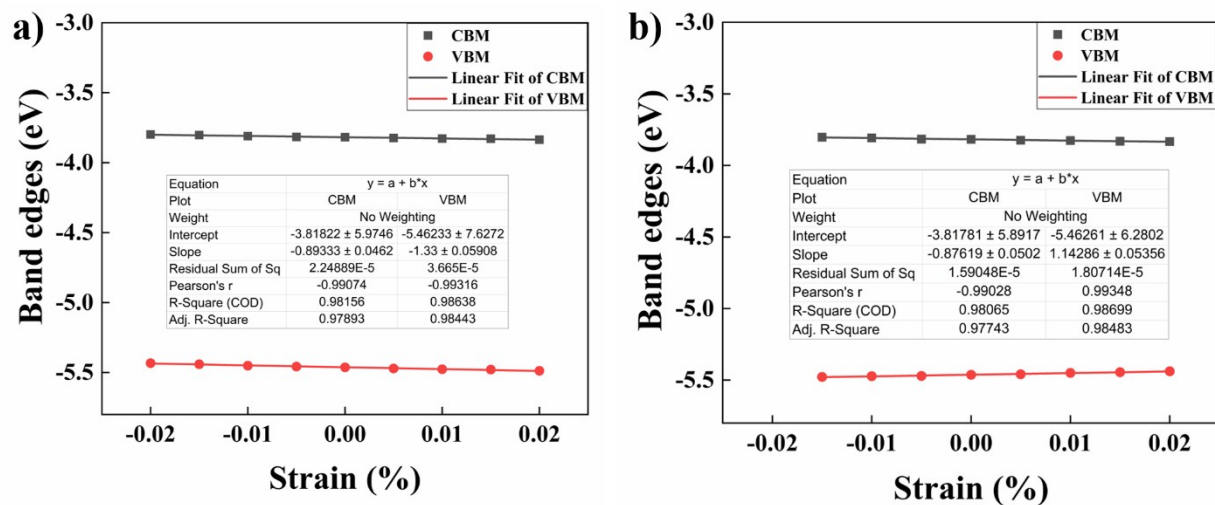

Fig S3: Deformation potential of BP/GaN along (a) zigzag and (b) armchair direction

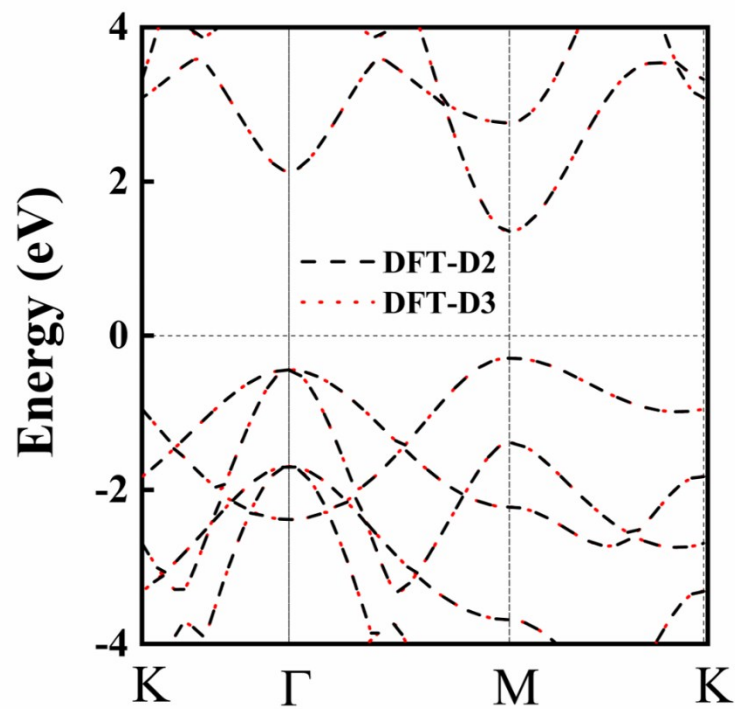Fig S4: Band structure of BP/GaN heterostructures with GGA-PBE incorporating DFT-D2/D3
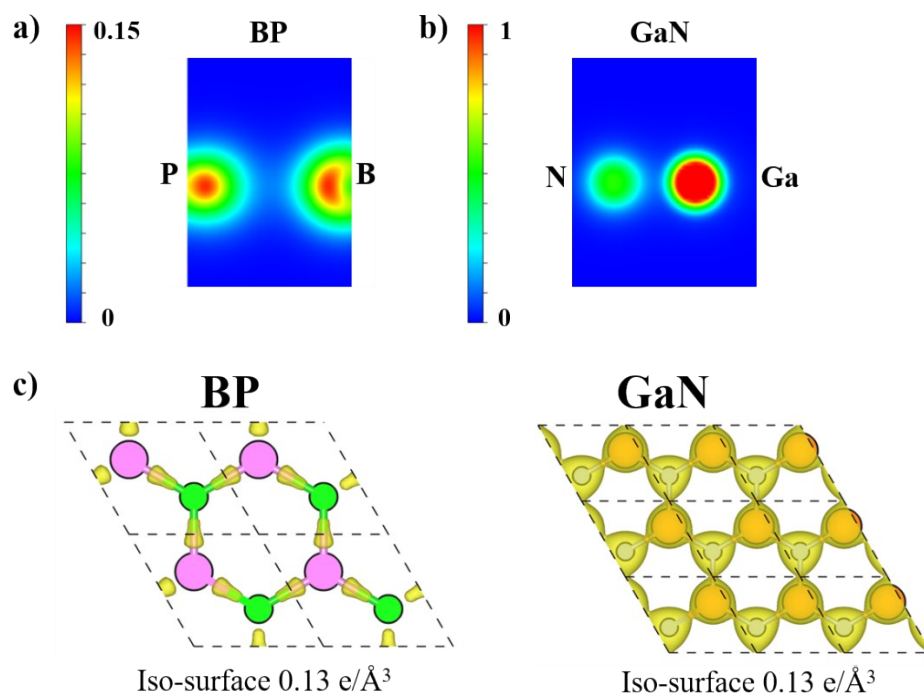

Iso-surface 0.13 e/Å³   Iso-surface 0.13 e/Å³
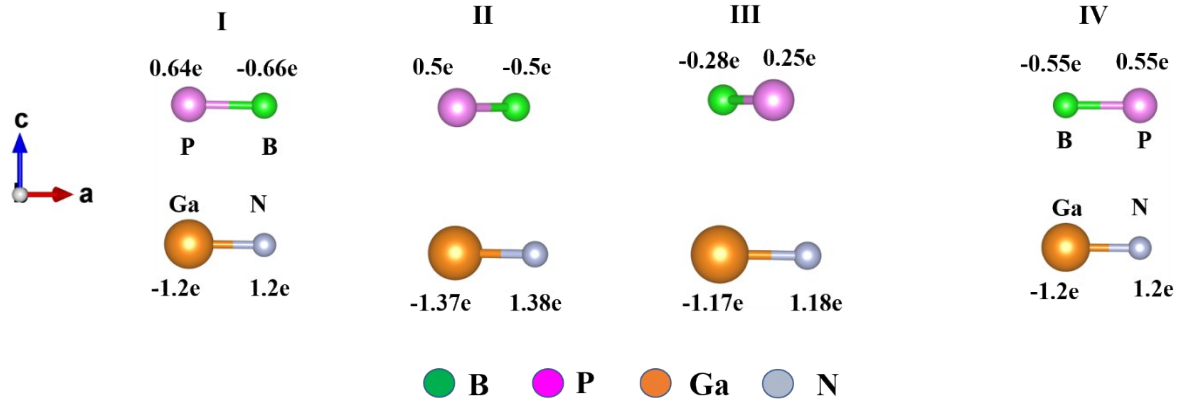
Fig S5: Charge density contour maps (e/Å³) for BP and GaN

Fig S6: Bader charge analysis of the heterostructure

Table-S1 Elastic constants of BP and GaN monolayer		C_{11} **(N/m)**	C_{12}**(N/m)**	Y **(N/m)**	v
BP	Our work	157.485	28.292	152.412	0.18
	Reported[1]	145.9	38.8	135.6	0.27
GaN	Our work	157.823	37.8	148.784	0.24

Table-S2 Effective mass (m*), deformation potential constant E$_i$ (eV) and carrier mobility μ (cm^{2}V^{-1}s^{-1}) for electrons and holes along high symmetric directions of BP and GaN monolayers at 300 K

System	Direction	Carrier type	$|m^*/m_o|$	$|E_i|$	μ (*10³) [Bardeen & Shockley]	μ (*10³) [Takagi]	μ (*10³) [Lang]
BP	$K \rightarrow \Gamma$	Electron	0.22	0.94	47.86	56.78	57.74
		Hole	0.21	2.45	7.5	9.57	9.39
	$K \rightarrow$ M	Electron	0.37	0.96	16.58	32.69	34.31
		Hole	0.31	2.62	3.1	5.8	6.2
GaN	$\Gamma \rightarrow M$	Electron	0.27[2]	1.45	14	21	23.23
	$K \rightarrow$ M	Hole	1.51	10.43	0.008	0.015	0.015
	$\Gamma \rightarrow K$	Electron	0.27	1.37	15.68	23.56	23.91
	$K \rightarrow \Gamma$	Hole	1.09	10.44	0.016	0.020	0.022

Our calculated values of electron and hole mobilities of monolayer BP are excellent agreement with the previously reported values.[3, 4]

Table-S3 Calculated ground state properties of the hetero-bilayer: equilibrium distance, potential drop Δ (eV), charge transfer ΔQ (e), binding energy (DFT-D3).

BP/GaN	h(Å)	Δ (eV)	|ΔQ| (e)	Binding energy DFT-D3 (meV/Å²)
II	3.27	1.18	0.055	17.2
III	3.29	0.70	0.074	16.26
IV	3.55	0.76	0.0078	12.4

Table-S4 Electronic/Ionic contribution of piezoelectric tensor (Cm^{-2}) and total elastic moduli (10^{10} GPa) of BP/GaN (I)

Electronic contribution:

Direction	XX	YY	ZZ
x	-0.00097	-0.00106	0.00027
y	-0.02249	0.02133	0.00016
z	0.00233	0.00229	0.00451

Ionic contribution:

Direction	XX	YY	ZZ
x	0.00056	-0.00058	0.00031
y	-0.07176	0.07175	0.00017
z	-0.00096	-0.00096	0.00746

Total Elastic Moduli (10^{10} Pa):

Direction	XX	YY	ZZ
XX	7.29	2.61	0.0064
YY	2.61	7.27	-0.0063
ZZ	0.006	-0.006	0.0285

Table S5 Born effective charges on each ionic species

	Orientation	Atoms	Born effective charges		
			XX	**YY**	**ZZ**
Pristine		Ga	3.08	3.08	0.33
		N	-3.08	-3.08	-0.33
		B	1.6	1.6	-0.02
		P	-1.6	-1.6	0.02
Heterobilayer	I	Ga	3.08	3.08	0.33
		N	-3.17	-3.17	-0.34
		B	1.862	1.86	0.056
		P	-1.773	-1.77	-0.04
	II	Ga	3.05	3.02	0.35
		N	-3.29	-3.17	-0.35
		B	1.63	1.42	-0.006
		P	-1.38	-1.27	0.008
	III	Ga	3.22	3.21	0.34
		N	-3.34	-3.28	-0.35
		B	2.06	1.97	0.004
		P	-1.94	-1.9	0.006
	IV	Ga	2.29	2.29	-0.37
		N	-2.71	-2.71	-0.37
		B	2.3	2.3	-0.07
		P	-2.54	-2.54	0.07

Photocatalytic water splitting:

Photocatalytic water splitting involves the production of electron and hole pairs upon absorption of solar energy. The photogenerated electrons participate in the hydrogen reduction reaction (eq 2) producing H_2 while the holes take part in the oxidation reaction (eq 1) to generate O_2.[5]

The photocatalytic process essentially consists of the following two reactions:

$$2H_2O + 4h^+ \rightarrow O_2 + 4H^+ \text{.........(1)}$$

$$2H^+ + 2e^- \rightarrow H_2 \text{..........(2)}$$
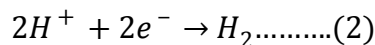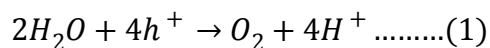
In addition to having a band gap > 1.23 eV, a semiconductor needs to have suitable VBM and CBM energy levels for the photocatalytic water splitting to be thermodynamically favorable: the VBM energy should be lower than the oxidation potential (-5.67 eV) of H_2O/O_2 in order to split first split and a CBM energy higher than the reduction potential (-4.44 eV) of H^+/H_2 to further produce H_2.[6] To evaluate photocatalytic ability we have checked the alignment of the band edges of our hetero structure with respect to standard water redox potentials, -5.67 eV and -4.44 eV, at zero pH in the normal hydrogen electrode (NHE) potential. Since GGA-PBE underestimate the bandgap, band edges have been calculated using HSE06 functional with respect to the absolute vacuum potential, as shown in Fig. S7. pH dependent redox potentials can be calculated using

$$E_{H^+/H_2}^{red} = -4.44\ eV + pH \times 0.059\ eV$$

for the standard reduction potential and

$$E_{O_2/H_2O}^{ox} = -5.67\ eV + pH \times 0.059\ eV$$

for oxidation potential.[7-10] The energy difference ΔE_1 between CBM level and water reduction potential and ΔE_2 between VBM and water oxidation potential (for pH = 0) are favorable enough to facilitate both hydrogen and oxygen evolution reactions, as shown in SI in Table-S6.
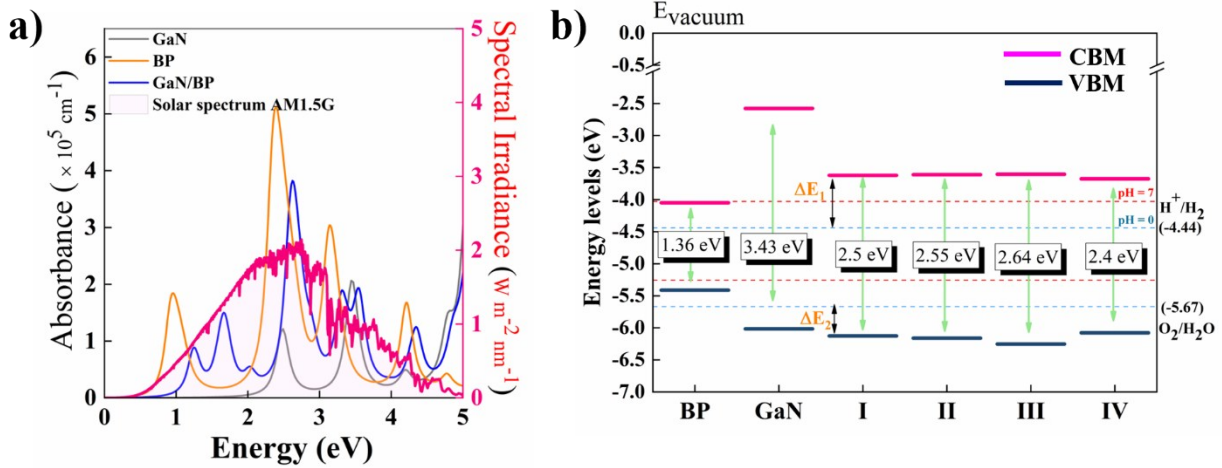

Figure S7. (a) The solar spectrum and calculated optical absorption spectra of monolayer GaN, BP and their heterobilayer (b) Band edge alignments of BP/GaN heterobilayer calculated using HSE06 as well as the water oxidation (O₂/H₂O) and reduction (H⁺/H₂) potential at pH= 0 (blue dash line) and pH=7 (red dash line)

Besides the need for the band edges to straddle the water redox potential, an efficient photocatalytic material should have a large absorbance in the solar energy spectrum. The optical absorption properties of heterobilayer are obtained by computing the complex dielectric function $\varepsilon(\omega) = \varepsilon_1(\omega) + i\varepsilon_2(\omega)$, where the imaginary part is related to the absorption at a given frequency ω. The absorption coefficient can be evaluated by the following formula[11],

$$\alpha_{abs} = \sqrt{2}\omega\left(\sqrt{\varepsilon_1^2(\omega) + \varepsilon_2^2(\omega)} - \varepsilon_1(\omega)\right)^{1/2} \dots\dots\dots\dots(3)$$

The imaginary part of the dielectric functions $\varepsilon_2(\omega)$ was calculated by summation over empty states while the real part $\varepsilon_1(\omega)$ was obtained by a Kramers-Kronig integration.[12, 13] Fig. 6 clearly shows the substantial absorption of heterobilayer in visible and UV light zone in comparison to that of the monolayers.

Under the effect of the synergy between band alignment and interlayer built-in potential, excitons are more likely to be dissociated into free electrons and holes. Smaller binding energy (E_b) promotes an easier splitting of excitons into free charge carriers. Thus, we have calculated exciton binding energy and exciton Bohr radius (a^*) from the Wannier-Mott model for 2D materials using the following equations:[14-18]

$$E_b = \frac{4\mu_{ex}}{m_0\varepsilon_r^2}R_H \ldots\ldots\ldots(4)$$

$$a^* = \frac{m_0}{4\mu_{ex}}\varepsilon_r a_H \ldots\ldots\ldots(5)$$

Where R_H, m_0 and μ are the Rydberg constant of a hydrogen atom (13.6 eV), free electron mass and effective reduced mass of an exciton respectively, a_H is the Bohr radius of the hydrogen atom. The macroscopic static dielectric tensor ε_r equals the sum of the electron contribution and ionic contribution, and has been obtained from the density functional perturbation theory. Stacking dependent exciton binding energy are listed in Table-5. The exciton binding energy of our heterobilayer are in the range of 0.6 − 1.5 eV which can be benchmarked against the exciton binding energy in MoS_2 (0.54 eV)[19] and C_3N_4 (0.33 eV)[17] respectively. The stacking order IV is found to favorably lower the exciton binding energies and hence, would be most suitable in solar energy harvesting.

Table-S6 Calculated excitonic effective mass, μ$_{ex}$ (m$_0$), macroscopic static dielectric constant (ε$_r$) and Exciton binding energy, E$_{exc}$ (eV) and excitonic Bohr radius, a^* (Å) for different stacking pattern labeled I-IV

BP/GaN	μ_{ex}		ε_r		E_{exc} (eV)		a^* (Å)	
	μ_{ex}^x	μ_{ex}^y	ε_r^x	ε_r^y	E_{exc}^x	E_{exc}^y	a_x^*	a_y^*
I	0.213	0.23	2.95	2.93	1.33	1.45	1.73	1.59
II	0.239	0.245	3.12	3.04	1.33	1.44	1.63	1.55
III	0.243	0.248	3.63	3.58	1	1.05	1.86	1.8
IV	0.184	0.199	3.93	3.93	0.65	0.7	2.66	2.46

Optimized structures of monolayers

POSCAR file (VASP format) of BP:

```
B P
   1.00000000000000
     3.2140967987598605    -0.0000000000000000     0.0000000000000000
    -1.6070483993799303     2.7834957138165146    -0.0000000000000000
     0.0000000000000000    -0.0000000000000000    27.0133087429363918
     B     P
     1     1
Selective dynamics
Direct
  0.6666672544959980   0.3333333006769976   0.5000510889686367     T   T   T
  0.3333327455040020   0.6666666993230024   0.4999489110313632     T   T   T
```

POSCAR file (VASP format) of GaN:

```
Ga N
   1.00000000000000
     3.2096369945226813   -0.0000000093815814    0.0000000000000000
    -1.6048235135107163    2.7796294050242207    0.0000000000000000
    -0.0000000000000000    0.0000000000000000   19.9953888000316020
    Ga    N
     1     1
Selective dynamics
Direct
  0.8333339681019964  0.6666664999999981  0.5000000000000000    T    T    T
  0.1666660318980036  0.3333335000000019  0.5000000000000000    T    T    T
```

References:

1.   D. Çakır, D. Kecik, H. Sahin, E. Durgun and F. M. Peeters, *Physical Chemistry Chemical Physics*, 2015, **17**, 13013-13020.
2.   R. Meng, J. Jiang, Q. Liang, Q. Yang, C. Tan, X. Sun and X. Chen, *Science China Materials*, 2016, **59**, 1027-1036.
3.   M. Xie, S. Zhang, B. Cai, Z. Zhu, Y. Zou and H. Zeng, *Nanoscale*, 2016, **8**, 13407-13413.
4.   B. Zeng, M. Li, X. Zhang, Y. Yi, L. Fu and M. Long, *The Journal of Physical Chemistry C*, 2016, **120**, 25037-25042.
5.   Q. Peng, Z. Guo, B. Sa, J. Zhou and Z. Sun, *International Journal of Hydrogen Energy*, 2018, **43**, 15995-16004.
6.   Y. Ji, M. Yang, H. Dong, T. Hou, L. Wang and Y. Li, *Nanoscale*, 2017, **9**, 8608-8615.
7.   Z. Ma, Z. Yi, J. Sun and K. Wu, *The Journal of Physical Chemistry C*, 2012, **116**, 25074-25080.
8.   S. Yao, X. Zhang, Z. Zhang, A. Chen and Z. Zhou, *International Journal of Hydrogen Energy*, 2019, **44**, 5948-5954.
9.   A. Huang, W. Shi and Z. Wang, *The Journal of Physical Chemistry C*, 2019, **123**, 11388-11396.
10.   X. Zhang, X. Zhao, D. Wu, Y. Jing and Z. Zhou, *Advanced Science*, 2016, **3**, 1600062.
11.   N. Miao, J. Zhou, B. Sa, B. Xu and Z. Sun, *Journal of Alloys and Compounds*, 2017, **699**, 554-560.
12.   M. Gajdoš, K. Hummer, G. Kresse, J. Furthmüller and F. Bechstedt, *Physical Review B*, 2006, **73**, 045112.
13.   S. Saha, T. P. Sinha and A. Mookerjee, *Physical Review B*, 2000, **62**, 8828-8834.
14.   X. Lv, W. Wei, Q. Sun, F. Li, B. Huang and Y. Dai, *Applied Catalysis B: Environmental*, 2017, **217**, 275-284.
15.   M. Dvorak, S.-H. Wei and Z. Wu, *Physical Review Letters*, 2013, **110**, 016402.
16.   G. Bastard, E. E. Mendez, L. L. Chang and L. Esaki, *Physical Review B*, 1982, **26**, 1974-1979.
17.   S. Melissen, T. Le Bahers, S. N. Steinmann and P. Sautet, *The Journal of Physical Chemistry C*, 2015, **119**, 25188-25196.
18.   X.-F. He, *Physical Review B*, 1991, **43**, 2063-2069.
19.   H. Shi, H. Pan, Y.-W. Zhang and B. I. Yakobson, *Physical Review B*, 2013, **87**, 155304.